L. Dozio
Refined 2-D Theories for Free Vibration Analysis of Annular Plates: Unified Ritz Formulation and Numerical Assessment
Computers & Structures, Vol. 147, 2015, p. 250-258
doi:10.1016/j.compstruc.2014.10.015

Refined 2-D theories for free vibration analysis of annular plates: unified Ritz formulation and numerical assessment

Lorenzo Dozio

Department of Aerospace Engineering
Politecnico di Milano
via La Masa, 34, 20156, Milan, Italy

Abstract

This paper presents a unified Ritz-based method for computation of modal properties of both thick and thin, circular and annular isotropic plates with different boundary conditions. The solution is based on an appropriate and simple formulation capable of handling in an unified way a large variety of two-dimensional higher-order plate theories. The formulation is also invariant with respect to the set of Ritz admissible functions. In this work, accurate upper-bound vibration solutions are presented by using kinematic models up to sixth order and products of Chebyshev polynomials and boundary-compliant functions. Considering the circumferential symmetry of annular plates and the 2-D nature of underlying theories, the present method is also computationally efficient since only single series of trial functions in the radial direction are required.

Keywords: free vibration analysis, circular and annular plates, higher-order plate theories, variable-kinematic Ritz method.

1 Introduction

Circular and annular plates are widely adopted as structural elements in many engineering fields. Therefore, reliable mathematical models capable of predicting with high accuracy their dynamic behaviour can be of great importance in the design process.

It is known that the accuracy in the computation of natural frequencies and mode shapes of plate structures can strongly depend on the kinematics assumed to represent their deformation. Modelling approaches range from fully three-dimensional (3-D) models, without any simplifying assumption on the kinematics of deformation, to traditional plate theories, like classical plate theory (CPT) and first-order shear deformation theory (FSDT), based on a reduction of the 3-D problem to simple and economical two-dimensional (2-D) models [1]. Many attempts lying in the middle have also appeared in the last three decades. They fall into the category of so-called refined or higher-order plate theories, where the conventional kinematics of FSDT is enriched with various higher-order terms as power series expansion of the thickness coordinate [2, 3, 4, 5, 6, 7, 8]. The aim of such refined theories is twofold. Firstly, to preserve the 2-D nature of the model and thus avoid the complexity and computational inefficiency of 3-D elasticity solutions. Secondly, to improve, compared to classical theories, the capability of estimating the correct mechanical behaviour of the plate when thickness-to-length ratio increases, accurate through-the-thickness distribution of displacements and stresses is sought or discrete medium-to-high frequency analysis is required.

In contrast to CPT and FSDT, plate theories of high order typically involve complicated mathematical formulations. Derivation and computer implementation of the corresponding models would be less cumbersome with the availability of appropriate techniques capable of handling in an easy and efficient way arbitrary refinements of classical theories. Furthermore, it would be highly desirable to rely on an unified modelling framework giving the ability of performing comparisons of different theories of increasing complexity without the need of a new modelling effort each time.

In view of the above remarks, this paper presents a unified Ritz-based formulation based on an entire class of 2-D higher-order theories for free vibration analysis of both thick and thin isotropic annular plates with different combinations of classical boundary conditions. The novelty of the present work is twofold.

Firstly, a comprehensive assessment of refined plate theories against free vibration of annular plates of any thickness is presented for the first time. Indeed, most of the past investigations on free vibration of circular and annular plates performed an exact or numerical analysis on the basis of CPT and FSDT (see, e.g., [9, 10, 11, 12, 13]). A satisfactory number of papers that carried out a 3-D vibration analysis are also available [14, 15, 16, 17, 18]. Conversely, probably due to the mathematical and computational complexities mentioned above, higher-order plate theories were employed only in very few works [19, 20, 21]. In particular, remarkable exact closed-form frequency solutions are obtained in [20] and [21] using Reddy's third-order shear deformation theory (TSDT). However, since TSDT discards thickness-stretching effects, which are increasingly important as the thickness-to-radius increases, their analysis is limited to moderately thick plates. The current study aims at evaluating how accurate natural frequencies of higher-order 2-D theories would be in representing a 3-D problem.

Secondly, all previous works on free vibration of circular and annular plates modelled according to 2-D theories suffer from a common shortcoming: they rely on axiomatic models with a fixed kinematic theory. As a result, the development of a refined theory of a certain order requires each time a new mathematical effort along with the related code implementation. This process can be cumbersome and prone to errors. The powerful yet simple method presented in the following overcomes the above deficiency.

The present study can be considered as an extension to annular plates of the variable-kinematic Ritz method developed in [22, 23, 24], which were focused on straight-sided quadrilateral plates. The formulation has some attractive properties. It is invariant with respect to both the specific plate theory and the set of admissible functions. In other words, a unified modelling framework is derived in terms of simple modelling kernels, called *Ritz fundamental nuclei*, which are properly expanded to yield the mass and stiffness matrices of the model. Considering the circumferential symmetry of circular plates and the 2-D nature of the underlying theories, the present method is also computationally efficient since only single series of trial functions in the radial direction are required. In addition, relying on a global approximation, the method has a high spectral accuracy and converges faster than local methods such as finite elements. As a result, the formulation derived in this work is accurate in providing benchmark values yet efficient to be used for design purposes and parametric analysis.

The current paper is an extended version of the conference paper [25] and includes a more complete numerical analysis with new comparison studies for plates with different thickness-to-radius ratios and boundary conditions. The paper is organised as follows. Section 2 contains the mathematical derivation of the method. Details about the Ritz trial set adopted in this study are also given. The convergence and numerical stability properties of the current approach are presented in Section 3. Upper-bound vibration solutions based on various higher-order 2-D models are shown in Section 4. In-depth discussion is provided by comparison the frequency parameters obtained by the current method with various results available in the literature. Finally, some concluding remarks are drawn in Section 5.

2 Theoretical formulation

An annular isotropic plate of outer radius R_o and inner radius R_i is considered as shown in Figure 1. The plate has uniform thickness h. An orthogonal cylindrical coordinate system is defined with radial direction r ($R_i \leq r \leq R_o$), circumferential direction θ ($0 \leq \theta \leq 2\pi$) and thickness direction z ($-h/2 \leq z \leq h/2$).

For generality and convenience, the present formulation is derived using a dimensionless coordinate ξ ($-1 \leq \xi \leq 1$) for the radial direction defined as follows

$$\xi = \frac{r}{\gamma} - \delta \tag{1}$$

where

$$\gamma = \frac{R_o - R_i}{2} \tag{2}$$

$$\delta = \frac{R_o + R_i}{R_o - R_i} \tag{3}$$

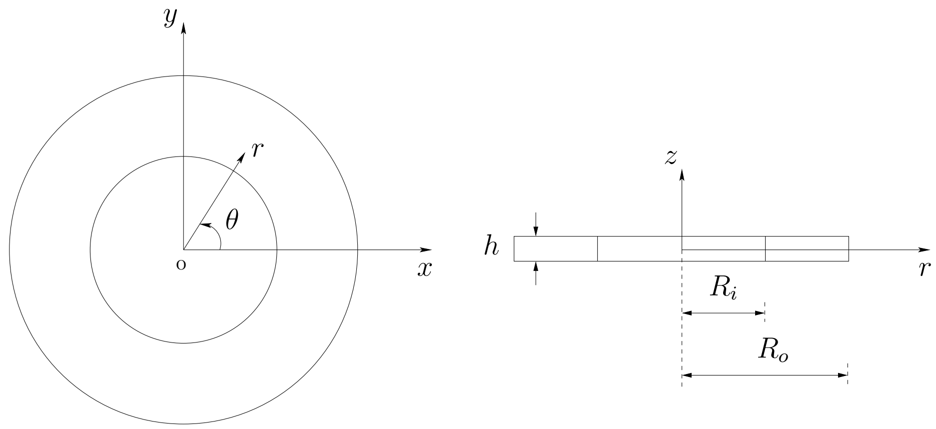

Figure 1: Geometry of an annular plate.

The displacement vector $\mathbf{u} = \mathbf{u}(\xi, \theta, z, t)$ of a generic point of the plate is given by

$$\mathbf{u}(\xi, \theta, z, t) = \left\{ \begin{array}{c} u_\xi(\xi, \theta, z, t) \\ u_\theta(\xi, \theta, z, t) \\ u_z(\xi, \theta, z, t) \end{array} \right\} \tag{4}$$

Strain components can be grouped into an in-plane strain vector $\boldsymbol{\varepsilon}_\mathrm{p}$ and out-of-plane (normal) strain vector $\boldsymbol{\varepsilon}_\mathrm{n}$ as follows

$$\boldsymbol{\varepsilon}_\mathrm{p} = \left\{ \begin{array}{c} \varepsilon_{\xi\xi} \\ \varepsilon_{\theta\theta} \\ \gamma_{\xi\theta} \end{array} \right\} \qquad \boldsymbol{\varepsilon}_\mathrm{n} = \left\{ \begin{array}{c} \gamma_{\xi z} \\ \gamma_{\theta z} \\ \varepsilon_{zz} \end{array} \right\} \tag{5}$$

Within the framework of linear, small strain, elasticity theory, strain vectors are related to displacements through the following equations

$$\boldsymbol{\varepsilon}_\mathrm{p} = \boldsymbol{D}_\mathrm{p}\mathbf{u} \tag{6}$$

$$\boldsymbol{\varepsilon}_\mathrm{n} = \boldsymbol{D}_\mathrm{n}\mathbf{u} + \boldsymbol{D}_z\mathbf{u} \tag{7}$$

where

$$\boldsymbol{D}_\mathrm{p} = \begin{bmatrix} \left(\frac{1}{\gamma}\right)\frac{\partial}{\partial\xi} & 0 & 0 \\ \left(\frac{1}{\gamma}\right)\frac{1}{\xi+\delta} & \left(\frac{1}{\gamma}\right)\frac{1}{\xi+\delta}\frac{\partial}{\partial\theta} & 0 \\ \left(\frac{1}{\gamma}\right)\frac{1}{\xi+\delta}\frac{\partial}{\partial\theta} & \left(\frac{1}{\gamma}\right)\left[\frac{\partial}{\partial\xi} - \frac{1}{\xi+\delta}\right] & 0 \end{bmatrix} \tag{8}$$

$$
\boldsymbol{D}_{\mathrm{n}} = \begin{bmatrix} 0 & 0 & \left(\dfrac{1}{\gamma}\right)\dfrac{\partial}{\partial \xi} \\ 0 & 0 & \left(\dfrac{1}{\gamma}\right)\dfrac{1}{\xi+\delta}\dfrac{\partial}{\partial \theta} \\ 0 & 0 & 0 \end{bmatrix} \tag{9}
$$

and

$$
\boldsymbol{D}_{z} = \mathrm{diag}\left[\frac{\partial}{\partial z}\right] \tag{10}
$$

Accordingly, the stress vector can be partitioned into in-plane $\boldsymbol{\sigma}_{\mathrm{p}}$ and out-of-plane $\boldsymbol{\sigma}_{\mathrm{n}}$ components. Using Eqs. (6) and (7), the three-dimensional Hooke's law can be written as

$$
\begin{aligned}
\boldsymbol{\sigma}_{\mathrm{p}} &= \mathbf{C}_{\mathrm{pp}}\boldsymbol{D}_{\mathrm{p}}\mathbf{u} + \mathbf{C}_{\mathrm{pn}}\boldsymbol{D}_{\mathrm{n}}\mathbf{u} + \mathbf{C}_{\mathrm{pn}}\boldsymbol{D}_{z}\mathbf{u} \\
\boldsymbol{\sigma}_{\mathrm{n}} &= \mathbf{C}_{\mathrm{np}}\boldsymbol{D}_{\mathrm{p}}\mathbf{u} + \mathbf{C}_{\mathrm{nn}}\boldsymbol{D}_{\mathrm{n}}\mathbf{u} + \mathbf{C}_{\mathrm{nn}}\boldsymbol{D}_{z}\mathbf{u}
\end{aligned} \tag{11}
$$

where the following matrices of stiffness coefficients are introduced:

$$
\begin{aligned}
\mathbf{C}_{\mathrm{pp}} &= \begin{bmatrix} C_{11} & C_{12} & 0 \\ C_{12} & C_{22} & 0 \\ 0 & 0 & C_{66} \end{bmatrix}, \quad \mathbf{C}_{\mathrm{pn}} = \begin{bmatrix} 0 & 0 & C_{13} \\ 0 & 0 & C_{23} \\ 0 & 0 & 0 \end{bmatrix} \\
\mathbf{C}_{\mathrm{np}} &= \begin{bmatrix} 0 & 0 & 0 \\ 0 & 0 & 0 \\ C_{13} & C_{23} & 0 \end{bmatrix}, \quad \mathbf{C}_{\mathrm{nn}} = \begin{bmatrix} C_{55} & 0 & 0 \\ 0 & C_{44} & 0 \\ 0 & 0 & C_{33} \end{bmatrix}
\end{aligned} \tag{12}
$$

In the case of isotropic materials, the elastic coefficients are given by

$$
\begin{aligned}
C_{11} = C_{22} = C_{33} &= \frac{E(1-\nu)}{(1+\nu)(1-2\nu)} \\
C_{12} = C_{13} = C_{23} &= \frac{E\nu}{(1+\nu)(1-2\nu)} \\
C_{44} = C_{55} = C_{66} = G &= \frac{E}{2(1+\nu)}
\end{aligned} \tag{13}
$$

in which E is the Young's modulus, ν is the Poisson's ratio, and G is the shear modulus.

According to the approach developed by Carrera [26], an entire class of two-dimensional higher-order plate theories can be compactly described through the following indicial notation:

$$
\mathbf{u}(\xi,\theta,z,t) = F_{\tau}(z)\mathbf{u}_{\tau}(\xi,\theta,t) \qquad (\tau = 0,1,\ldots,N) \tag{14}
$$

where $\mathbf{u}_{\tau}(\xi,\theta,t)$ is the displacement vector containing the unknown kinematic variables related to the specific plate theory, τ is an integer index related to the order N of the theory and $F_{\tau}(z)$ are selected functions in the thickness direction. The summation convention on indices appearing twice is implied in Eq. (14). In this work, the z

expansion is implemented via Taylor polynomials. For the sake of brevity, a higher-order theory of order N will be indicated in the following by HOT_N. For example, HOT_3 is a plate theory of order 3 based on the following assumed kinematic field:

$$\begin{aligned} u_\xi &= u_{\xi 0} + z u_{\xi 1} + z^2 u_{\xi 2} + z^3 u_{\xi 3} \\ u_\theta &= u_{\theta 0} + z u_{\theta 1} + z^2 u_{\theta 2} + z^3 u_{\theta 3} \\ u_z &= u_{z0} + z u_{z1} + z^2 u_{z2} + z^3 u_{z3} \end{aligned}$$

The total number of kinematic degrees of freedom for a given HOT_N is $3\,(N+1)$. Note that the consideration of higher-order terms in u_z allows the inclusion in the present formulation of thickness-stretching effects.

Assuming a harmonic motion and considering the circumferential symmetry of the plate about the coordinate θ, the displacements can be expressed as

$$\mathbf{u}(\xi,\theta,z,t) = F_\tau(z) \left\{ \begin{array}{c} \hat{u}_{\xi\tau}(\xi)\cos{(n\theta)} \\ \hat{u}_{\theta\tau}(\xi)\sin{(n\theta)} \\ \hat{u}_{z\tau}(\xi)\cos{(n\theta)} \end{array} \right\} e^{j\omega t} \tag{15}$$

or, in matrix form,

$$\mathbf{u}(\xi,\theta,z,t) = F_\tau(z)\boldsymbol{\Theta}(n\theta)\hat{\mathbf{u}}_\tau(\xi)e^{j\omega t} \tag{16}$$

where $\hat{u}$'s are amplitude functions of the dimensionless radial coordinate, $n = 0, 1, 2, \ldots$ is the circumferential wavenumber and $\boldsymbol{\Theta}(n\theta) = \mathrm{diag}(\cos n\theta, \sin n\theta, \cos n\theta)$. Note that $n = 0$ in Eq. (15) yields axisymmetric vibration which involves only u_ξ and u_z. A complementary displacement field can be also used by replacing $\cos(n\theta)$ by $\sin(n\theta)$, and conversely, in Eq. (15). In this case, torsional vibration modes are obtained when $n = 0$.

A standard Ritz solution is sought for each component of the displacement vector $\hat{\mathbf{u}}_\tau(\xi)$ as follows

$$\begin{aligned} \hat{u}_{\xi\tau}(\xi) &= \phi_{\xi\tau i}(\xi)c_{\xi\tau i} \\ \hat{u}_{\theta\tau}(\xi) &= \phi_{\theta\tau i}(\xi)c_{\theta\tau i} \qquad\qquad (i = 1, 2, \ldots, M) \\ \hat{u}_{z\tau}(\xi) &= \phi_{z\tau i}(\xi)c_{z\tau i} \end{aligned} \tag{17}$$

where M is the order of the Ritz expansion, $c_{\alpha\tau i}$ ($\alpha = \xi, \theta, z$) are the unknown Ritz coefficients, and $\phi_{\alpha\tau i}$ are the corresponding Ritz trial functions. Note that, as before for the theory-related index τ in Eq. (14), Ritz-related dummy index i in Eq. (17) implies summation. The i-th admissible function $\phi_{\alpha\tau i}(\xi)$ is chosen here as the product of boundary-compliant functions and the one-dimensional Chebyshev polynomial [17]:

$$\phi_{\alpha\tau i}(\xi) = f_{\alpha\tau}^{\mathrm{inn}}(\xi) f_{\alpha\tau}^{\mathrm{out}}(\xi)\cos{[(i-1)\arccos(\xi)]} \tag{18}$$

where $f_{\alpha\tau}^{\mathrm{inn}}(\xi)$ and $f_{\alpha\tau}^{\mathrm{out}}(\xi)$ enable the displacement component $u_{\alpha\tau}$ to satisfy the geometric boundary conditions at the inner ($\xi = -1$) and outer ($\xi = +1$) edges of the plate, respectively. The boundary functions corresponding to the most common boundary conditions are reported in Table 1. It is clear that $f_{\alpha\tau}^{\mathrm{inn}}(\xi) = 1$ in the case

Boundary condition	$f_{\xi\tau}^{\mathrm{inn}}$	$f_{\theta\tau}^{\mathrm{inn}}$	$f_{z\tau}^{\mathrm{inn}}$	$f_{\xi\tau}^{\mathrm{out}}$	$f_{\theta\tau}^{\mathrm{out}}$	$f_{z\tau}^{\mathrm{out}}$
Clamped	$1+\xi$	$1+\xi$	$1+\xi$	$1-\xi$	$1-\xi$	$1-\xi$
Hard simply supported	1	$1+\xi$	$1+\xi$	1	$1-\xi$	$1-\xi$
Soft simply supported	1	1	$1+\xi$	1	1	$1-\xi$
Free	1	1	1	1	1	1

Table 1: Boundary functions.

of a solid circular plate. Chebyshev polynomials form a complete and orthogonal set in the interval $[-1, +1]$. As such, good convergence and numerical stability of the method are expected.

For the sake of compact notation, Eq. (17) is rearranged in matrix form as follows

$$\hat{\mathbf{u}}_\tau(\xi) = \mathbf{\Phi}_{\tau i}(\xi)\mathbf{c}_{\tau i} \tag{19}$$

where $\mathbf{\Phi}_{\tau i}(\xi) = \mathrm{diag}(\phi_{\xi\tau i}, \phi_{\theta\tau i}, \phi_{z\tau i})$ and $\mathbf{c}_{\tau i} = \{c_{\xi\tau i} \quad c_{\theta\tau i} \quad c_{z\tau i}\}^T$. Therefore, the displacement vector in Eq. (16) is given by

$$\mathbf{u}(\xi, \theta, z, t) = F_\tau(z)\mathbf{\Theta}(n\theta)\mathbf{\Phi}_{\tau i}(\xi)\mathbf{c}_{\tau i}e^{j\omega t} \tag{20}$$

The potential and kinetic energy of the plate are expressed, respectively, as

$$U = \frac{1}{2}\gamma^2 \int_{-1}^{+1}\int_{0}^{2\pi}\int_{-\frac{h}{2}}^{+\frac{h}{2}} \left(\boldsymbol{\varepsilon}_\mathrm{p}^T\mathbf{C}_\mathrm{pp}\boldsymbol{\varepsilon}_\mathrm{p} + \boldsymbol{\varepsilon}_\mathrm{p}^T\mathbf{C}_\mathrm{pn}\boldsymbol{\varepsilon}_\mathrm{n} + \boldsymbol{\varepsilon}_\mathrm{n}^T\mathbf{C}_\mathrm{np}\boldsymbol{\varepsilon}_\mathrm{p} + \boldsymbol{\varepsilon}_\mathrm{n}^T\mathbf{C}_\mathrm{nn}\boldsymbol{\varepsilon}_\mathrm{n}\right)(\xi+\delta)\,\mathrm{d}z\mathrm{d}\theta\mathrm{d}\xi \tag{21}$$

and

$$T = \frac{1}{2}\gamma^2 \int_{-1}^{+1}\int_{0}^{2\pi}\int_{-\frac{h}{2}}^{+\frac{h}{2}} \rho\left[\left(\frac{\partial u_\xi}{\partial t}\right)^2 + \left(\frac{\partial u_\theta}{\partial t}\right)^2 + \left(\frac{\partial u_z}{\partial t}\right)^2\right](\xi+\delta)\mathrm{d}z\mathrm{d}\theta\mathrm{d}\xi \tag{22}$$

where ρ is the mass density of the plate. Substituting Eq. (20) into Eqs. (6) and (7) and using Hooke's law in Eq. (11), the expressions of the maximum potential and kinetic energy of the plate vibrating harmonically can be compactly written as follows:

$$U_\mathrm{max} = \frac{1}{2}\mathbf{c}_{\tau i}^T\mathbf{K}_{\tau sij}\mathbf{c}_{sj} \tag{23}$$

and

$$T_\mathrm{max} = \frac{1}{2}\omega^2\mathbf{c}_{\tau i}^T\mathbf{M}_{\tau sij}\mathbf{c}_{sj} \tag{24}$$

where s and j are other theory-related and Ritz-related dummy indices, respectively.

In the above equations, when $n \neq 0$, $\mathbf{K}_{\tau sij}$ and $\mathbf{M}_{\tau sij}$ are 3×3 matrices given by

$$\begin{aligned}\mathbf{K}_{\tau sij} = \gamma^2 \int_{-1}^{+1} \int_{0}^{2\pi} \Big\{ & \left[\boldsymbol{D}_\mathrm{p} \boldsymbol{\Theta}(n\theta) \boldsymbol{\Phi}_{\tau i}(\xi)\right]^T \left[\mathbf{Z}^{\mathrm{pp}}_{\tau s} \boldsymbol{D}_\mathrm{p} + \mathbf{Z}^{\mathrm{pn}}_{\tau s} \boldsymbol{D}_\mathrm{n} \right. \\ & \left. + \mathbf{Z}^{\mathrm{pn}}_{\tau s_{,z}} \right] \boldsymbol{\Theta}(n\theta) \boldsymbol{\Phi}_{sj}(\xi) + \left[\boldsymbol{D}_\mathrm{n} \boldsymbol{\Theta}(n\theta) \boldsymbol{\Phi}_{\tau i}(\xi)\right]^T \left[\mathbf{Z}^{\mathrm{np}}_{\tau s} \boldsymbol{D}_\mathrm{p} \right. \\ & \left. + \mathbf{Z}^{\mathrm{nn}}_{\tau s} \boldsymbol{D}_\mathrm{n} + \mathbf{Z}^{\mathrm{nn}}_{\tau s_{,z}} \right] \boldsymbol{\Theta}(n\theta) \boldsymbol{\Phi}_{sj}(\xi) + \left[\boldsymbol{\Theta}(n\theta) \boldsymbol{\Phi}_{\tau i}(\xi)\right]^T \left[\mathbf{Z}^{\mathrm{np}}_{\tau_{,z} s} \boldsymbol{D}_\mathrm{p} \right. \\ & \left. + \mathbf{Z}^{\mathrm{nn}}_{\tau_{,z} s} \boldsymbol{D}_\mathrm{n} + \mathbf{Z}^{\mathrm{nn}}_{\tau_{,z} s_{,z}} \right] \boldsymbol{\Theta}(n\theta) \boldsymbol{\Phi}_{sj}(\xi) \Big\} (\xi + \delta)\, \mathrm{d}\theta \mathrm{d}\xi \end{aligned} \tag{25}$$

and

$$\mathbf{M}_{\tau sij} = \gamma^2 \int_{-1}^{+1} \int_{0}^{2\pi} \left[\boldsymbol{\Theta}(n\theta) \boldsymbol{\Phi}_{\tau i}(\xi)\right]^T \mathbf{Z}^{\rho}_{\tau s} \boldsymbol{\Theta}(n\theta) \boldsymbol{\Phi}_{sj}(\xi)\, (\xi + \delta)\, \mathrm{d}\theta \mathrm{d}\xi \tag{26}$$

where $\mathbf{Z}^{\mathrm{pp}}_{\tau s}, \ldots, \mathbf{Z}^{\rho}_{\tau s}$ are matrices of thickness integrals whose expression is given in Appendix A. Matrices in Eqs. (25) and (26) represent modeling kernels and are called *Ritz fundamental nuclei* of the present formulation. Indeed, they are invariant with respect to both the underlying kinematic theory and the set of Ritz admissible functions. In the case of axisymmetric modes, the condition $n = 0$ yields fundamental nuclei $\mathbf{K}_{\tau sij}$ and $\mathbf{M}_{\tau sij}$ of dimension 2×2 since only u_ξ and u_z are involved. In the case of torsional vibration, the fundamental nuclei reduce to scalar quantities. The elements of $\mathbf{K}_{\tau sij}$ and $\mathbf{M}_{\tau sij}$ are explicitly reported in Appendix B.

The stiffness and mass matrices of the plate are built from the above nuclei through an assembly-like procedure. The nuclei are first expanded to $3(N+1) \times 3(N+1)$ matrices by varying the theory-related indices τ and s from 0 to N. This expansion yields

$$\mathbf{K}_{ij} = \begin{bmatrix} \mathbf{K}_{00ij} & \mathbf{K}_{0rij} & \mathbf{K}_{0Nij} \\ \mathbf{K}_{r0ij} & \mathbf{K}_{rrij} & \mathbf{K}_{rNij} \\ \mathbf{K}_{N0ij} & \mathbf{K}_{Nrij} & \mathbf{K}_{NNij} \end{bmatrix} \tag{27}$$

$$\mathbf{M}_{ij} = \begin{bmatrix} \mathbf{M}_{00ij} & \mathbf{M}_{0rij} & \mathbf{M}_{0Nij} \\ \mathbf{M}_{r0ij} & \mathbf{M}_{rrij} & \mathbf{M}_{rNij} \\ \mathbf{M}_{N0ij} & \mathbf{M}_{Nrij} & \mathbf{M}_{NNij} \end{bmatrix} \tag{28}$$

where $r = 1, \ldots, N-1$. Then, the final matrices $\mathbf{K}$ and $\mathbf{M}$ of dimensions $3M(N+1) \times 3M(N+1)$ are generated accordingly through variation of Ritz-related indeces i and j in the above quantities $\mathbf{K}_{ij}$ and $\mathbf{M}_{ij}$ and by applying the same assembly operations adopted for the nuclei expansion.

The extremization of the energy functional $\Pi = U_{\max} - T_{\max}$ with respect to the coefficients $\mathbf{c}_{\tau i}$ yields the following generalized eigenvalue problem:

$$\left(\mathbf{K} - \omega^2 \mathbf{M}\right) \mathbf{c} = \mathbf{0} \tag{29}$$

where $\mathbf{c}$ is the vector containing the unknown coefficients $\mathbf{c}_{sj}$.

3 Convergence and stability analysis

The mathematically complete set of admissible functions in Eq. (18) yields upper-bound frequency values with increasing accuracy towards exact solutions as the number of terms M retained in the series of Eq. (19) increases. However, nothing can be said in advance with regard to the efficiency of the present method in terms of rate of convergence. Furthermore, possible numerical issues associated with ill-conditioned eigenvalue problems in Eq. (29) can arise when an high number of terms are taken.

3.1 Convergence study

The convergence of the method is discussed by referring to the particular case of a clamped solid circular plate ($R_o = R$) with various thickness-to-radius h/R ratios. It is worth noting that the conclusions outlined in the following are also valid for circular plates with other boundary conditions and for annular plates having different R_o/R_i ratios. Clamping boundary conditions have been selected since the convergence is expected to be slower than for other edge conditions, even for the lowest frequency parameters [15, 22]. This is mainly due to the difficulty of global trial functions in approximating the actual displacement field near the fixed boundary. Three cases are considered corresponding to a thin plate ($h/R = 0.01$), a moderately thick plate ($h/R = 0.1$), and a very thick plate ($h/R = 0.5$). The first six non-dimensional frequencies $\lambda = \omega R^2\sqrt{\rho h/D}$, where $D = Eh^3/12(1-\nu^2)$ is the plate bending stiffness, are listed in Table 2 for three different kinematic theories of increasing complexity ($N = 1, 2, 6$). Numerical results are shown as functions of increasing value of order M for the Ritz expansion in the radial direction. Frequency values with superscripts a and t denote axisymmetric and torsional vibration modes, respectively, corresponding to $n = 0$. In the following, Poisson's ratio is taken as $\nu = 0.3$.

As expected, all the frequency parameters monotonically decrease with the increase in the number of admissible functions, regardless of the thickness-to-radius ratio and the order of the kinematic model.

For each thickness-to-radius ratio, the rate of convergence of the method is very similar for HOT_2 and HOT_6. Although corresponding results are not shown here due to brevity reasons, the same can be said for kinematic models of intermediate order. From Table 2, it can be seen that fewer terms are needed for the frequency values to converge when the thickness dimension becomes significant. Indeed, all the first six frequency parameters converged to five-digit upper-bound values with $M = 16$ in the case of $h/R = 0.5$. When thinner plates are considered, the same frequencies are of only three- or four-digit accuracy even when the order M raises up to 30. A more rapid convergence as the plate thickness ratio increases has been also observed in 3-D Ritz-based vibration studies [16]. Moreover, the substantial invariance of the convergence behavior with respect to the assumed kinematic theory was also found in previous works on straight-sided plates [22, 23].

By further comparing solutions obtained with $N = 2$ with those obtained with $N =$

Table 2: Convergence of the first six frequency parameters $\lambda = \omega R^2 \sqrt{\rho h/D}$ for solid clamped circular plates.

			Mode					
N	h/R	M	1	2	3	4	5	6
1	0.01	8	11.304^a	23.518	38.568	43.976^a	56.410	67.232
		10	11.304	23.518	38.568	43.976	56.409	67.229
		20	11.304	23.518	38.568	43.976	56.409	67.229
	0.1	8	11.000^a	22.324	35.625	40.354^a	50.625	59.557
		10	11.000	22.324	35.625	40.354	50.624	59.556
		20	11.000	22.324	35.625	40.354	50.624	59.556
	0.5	8	7.3607^a	12.364	13.720	15.705^t	17.387	19.102^a
		10	7.3607	12.364	13.720	15.705	17.387	19.102
		18	7.3607	12.364	13.720	15.705	17.387	19.102
2	0.01	8	10.259^a	21.345	35.006	39.916^a	51.201	61.022
		10	10.244	21.314	34.955	39.858	51.129	60.938
		20	10.222	21.269	34.881	39.773	51.019	60.808
		30	10.218	21.260	34.867	39.757	50.999	60.783
		40	10.217	21.257	34.862	39.752	50.992	60.775
	0.1	8	10.030^a	20.426	32.713	37.085^a	46.647	54.963
		10	10.019	20.404	32.679	37.048	46.602	54.912
		20	10.010	20.386	32.652	37.018	46.566	54.870
		30	10.010	20.386	32.652	37.018	46.565	54.869
	0.5	8	7.0527^a	11.955	13.684	15.705^t	16.864	18.548^a
		10	7.0525	11.955	13.684	15.705	16.864	18.547
		16	7.0525	11.955	13.684	15.705	16.864	18.547
		18	7.0525	11.955	13.684	15.705	16.864	18.547
6	0.01	8	10.258^a	21.343	35.003	39.912^a	51.194	61.013
		10	10.243	21.312	34.952	39.853	51.122	60.928
		20	10.222	21.267	34.877	39.768	51.012	60.798
		30	10.217	21.258	34.863	39.752	50.991	60.773
		40	10.216	21.255	34.858	39.747	50.984	60.765
	0.1	8	9.9973^a	20.310	32.449	36.766^a	46.167	54.340
		10	9.9862	20.288	32.416	36.728	46.121	54.286
		20	9.9746	20.265	32.381	36.689	46.073	54.230
		30	9.9735	20.263	32.377	36.685	46.068	54.224
	0.5	8	6.8094^a	11.501	13.659	15.705^t	16.234	17.829^a
		10	6.8075	11.498	13.657	15.705	16.231	17.827
		16	6.8060	11.497	13.657	15.705	16.230	17.825
		18	6.8060	11.497	13.657	15.705	16.230	17.825

6, it is noted that, except for the thin case ($h/R = 0.01$) and the results corresponding to torsional modes, all the natural frequencies converged to different values according to the adopted theory. As shown in the next section, the accuracy of the solution for moderately thick and very thick plates is largely affected by the underlying kinematic model. In the case of thin plates, frequency values computed by plate theories of increasing order are all very close to each other and completely consistent with results obtained from the classical 2-D Kirchhoff theory (see Table 2.1 in [9]).

Tabulated results corresponding to $N = 1$ show that the rate of convergence of the method is very fast in that case, regardless of the thickness-to-radius ratio. All the frequency parameters converged to five-digit upper-bound values with $M = 10$. However, it is observed that convergent results are all significantly higher than those obtained with more refined theories. This behavior is due to a locking mechanism, known as thickness locking (TL), which occurs when the kinematic model exhibits a constant distribution of the transverse normal strain ε_{zz} [22]. Note that TL effects are more distinct for thin plates and bending dominated modes and slightly decrease with increasing thickness. A way to avoid TL when a first-order theory is used is discussed in the next section.

3.2 Numerical stability

As far as the numerical stability of the method is concerned, it can be noticed from Table 2 that ill-conditioning of the eigenvalue problem is avoided even when a high number M of terms is taken to compute the frequency solutions. Indeed, it is shown in Table 2 that stable numerical analysis can still be carried out when $M = 40$.

As a further insight, a numerical test involving up to $M = 100$ terms in the radial direction is presented in Table 3 by referring again to a clamped circular plate. Only the thin case with $h/R = 0.01$ is now considered. Some selected frequency parameters $\lambda = \omega R^2 \sqrt{\rho h/D}$ corresponding to vibration modes with $n = 1$ and different radial mode numbers $s = 1, 5, 10, 15, 20, 25$ are tabulated using a refined theory of fourth order ($N = 4$). It is observed that stable solutions are obtained for both low and high values of radial wavenumbers. As shown in the table, such immunity against ill-conditioned behavior can be of great importance in improving the accuracy of the eigenfrequencies of higher order vibration modes.

4 Numerical assessment

The variable-kinematic Ritz formulation derived in Section 2 is here validated against some reference solutions available in the literature. In particular, the following analysis is focused on comparing eigenfrequencies of different annular plates obtained on the basis of higher-order 2-D theories with those computed using a fully 3-D approach. Some results are given in tabulated form, so that listed solutions may serve as benchmark values for future comparison.

Table 3: Convergence and numerical stability of modes corresponding to $n = 1$ and different radial mode numbers s for a solid clamped circular plate with $h/R = 0.01$ using HOT_4.

	s					
M	1	5	10	15	20	25
10	21.3124	301.531	1487.54	3053.78	5442.73	9136.66
20	21.2670	296.267	876.225	1734.88	2952.54	4338.17
30	21.2582	296.144	875.737	1734.85	2399.24	3232.13
40	21.2555	296.108	875.633	1734.84	2399.24	3189.49
50	21.2547	296.097	875.599	1734.84	2399.24	3189.38
60	21.2544	296.092	875.585	1734.84	2399.24	3189.33
70	21.2542	296.090	875.578	1734.84	2399.24	3189.31
80	21.2541	296.089	875.575	1734.84	2399.24	3189.29
90	21.2541	296.088	875.574	1734.84	2399.24	3189.29
100	21.2541	296.088	875.573	1734.84	2399.24	3189.29

Table 4: Frequency parameters $\lambda = \omega R_o^2 \sqrt{\rho h/D}$ for the first eight modes of annular plates with $R_o = (10/3)R_i$, $h/R_o = 0.2$ and various boundary conditions (BCs).

		Mode							
BCs	Method	1	2	3	4	5	6	7	8
FS	Present ($N = 1$)	4.9611	12.171	12.761	15.942	22.959	27.961	32.928	33.166
	Present ($N = 2$)	4.5470	11.365	12.744	15.907	21.107	27.933	31.059	32.042
	Present ($N = 3$)	4.5401	11.240	12.743	15.906	20.856	27.932	30.717	31.553
	Present ($N = 4$)	4.5399	11.240	12.741	15.904	20.852	27.931	30.709	31.543
	Present ($N = 5$)	4.5398	11.239	12.740	15.904	20.852	27.931	30.708	31.542
	Present ($N = 6$)	4.5398	11.239	12.740	15.904	20.852	27.931	30.708	31.542
	3D-Ritz [16]	4.5401	11.240	12.742	15.904	20.852	27.931	30.709	31.543
FF	Present ($N = 1$)	4.7487	8.5204	11.462	15.687	16.290	19.438	27.918	28.378
	Present ($N = 2$)	4.6393	7.9075	11.222	15.389	15.662	19.030	27.206	27.779
	Present ($N = 3$)	4.6196	7.8940	11.143	15.189	15.662	18.828	26.815	27.384
	Present ($N = 4$)	4.6196	7.8939	11.143	15.187	15.661	18.826	26.809	27.378
	Present ($N = 5$)	4.6195	7.8939	11.143	15.187	15.661	18.826	26.808	27.377
	Present ($N = 6$)	4.6195	7.8939	11.143	15.187	15.661	18.826	26.808	27.377
	3D-Ritz [16]	4.6198	7.8939	11.143	15.189	15.662	18.826	26.810	27.378
FC	Present ($N = 1$)	11.143	17.069	27.808	39.482	39.662	39.964	40.534	44.172
	Present ($N = 2$)	10.553	16.323	26.210	37.101	38.249	39.627	40.534	44.106
	Present ($N = 3$)	10.453	16.035	25.674	36.263	37.403	39.606	40.534	44.083
	Present ($N = 4$)	10.442	16.020	25.645	36.214	37.339	39.598	40.534	44.074
	Present ($N = 5$)	10.440	16.015	25.638	36.202	37.321	39.594	40.534	44.071
	Present ($N = 6$)	10.438	16.013	25.634	36.197	37.313	39.592	40.534	44.068
	3D-Ritz [16]	10.448	16.026	25.650	36.220	37.346	39.602	–	44.080
	3D-Ritz [17]	10.437	16.012	25.632	36.194	37.309	39.591	40.534	44.066
CC	Present ($N = 1$)	33.182	33.965	37.123	43.579	48.220	52.792	53.107	63.563
	Present ($N = 2$)	31.822	32.548	35.451	41.442	48.220	50.147	53.085	60.479
	Present ($N = 3$)	30.835	31.565	34.456	40.353	48.220	48.835	53.075	58.844
	Present ($N = 4$)	30.741	31.473	34.371	40.271	48.220	48.745	53.071	58.729
	Present ($N = 5$)	30.711	31.444	34.344	40.248	48.220	48.722	53.069	58.704
	Present ($N = 6$)	30.696	31.430	34.333	40.238	48.220	48.713	53.068	58.695
	3D-Ritz [16]	30.743	31.474	34.370	40.266	–	48.736	53.072	–
	3D-Ritz [17]	30.688	31.422	34.325	40.231	48.220	48.707	53.067	58.689

The first analysis is referred to annular plates with $R_o = (10/3)R_i$ and $h/R_o = 0.2$. Four cases with different combinations of free (F), clamped (C) and hard simply supported (S) boundary conditions are considered. For the sake of brevity, a two-letter symbolic notation is used to define the conditions at the inner and outer edges, respectively. The first eight frequency parameters $\lambda = \omega R_o^2 \sqrt{\rho h/D}$ are sorted in Table 4 as a result of the adoption of kinematic models of order $N = 1, \dots, 6$. Present Ritz-based solutions are computed with $M = 30$ and compared with those obtained from three-dimensional analysis using orthogonally generated polynomial functions [16] and Chebyshev polynomials [17]. Note that missing terms corresponding to mode 7th and mode 5th for FC and CC boundary conditions, respectively, are related to a torsional mode, which was not computed in [16]. Instead, missing term corresponding to mode 8th for the case of inner and outer edges clamped is not reported by Liew and Yang [16]. The following observations can be made from computed results.

First, it is clear from Table 4 that frequency values arising from 2-D models converge towards 3-D based accurate solutions reported in [16, 17] as the order N of the underlying theory increases. The agreement is excellent when computations are performed using a kinematic model of order 6. The accuracy is slightly worse, but still very good, for models of lower order. This shows that, using the variable-kinematic formulation presented in this work, one can easily select the theory refinement needed to achieve a desired accuracy without any further development effort and without the complexity and computational inefficiency associated to 3-D models.

Note also that upper-bound results obtained by the present method using $N \geq 4$ are slightly lower than those obtained in [16] from a 3-D analysis. This is probably due to the relatively low number of Ritz terms taken in the radial and thickness directions in the 3-D case.

As a third remark, it is found that the accuracy in the computation of natural frequencies corresponding to torsional modes is not affected by the assumed plate theory and the computed solutions coincide with 3-D values.

Finally, contrary to theories of higher order where at least a parabolic distribution of transverse displacement component u_z is adopted, it is observed that frequency solutions based on HOT_1 suffer from the already mentioned effects due to thickness locking. A known technique to contrast TL consists of modifying the elastic stiffness coefficients by imposing the condition $\sigma_{zz} = 0$. In this way, the first-order shear deformation theory can be actually obtained from HOT_1 using the present formulation. The reduced elastic coefficients in Eq. (11) are the following

$$\begin{aligned} \tilde{C}_{ij} &= C_{ij} - \frac{C_{i3}C_{j3}}{C_{33}} \quad (i, j = 1, 2) \\ \tilde{C}_{ii} &= \chi C_{ii} \quad (i = 4, 5) \end{aligned} \tag{30}$$

where χ is the shear correction factor. Frequency parameters obtained with imposition of $\sigma_{zz} = 0$ in HOT_1 for the same annular plate previously considered are reported in Table 5. Results are computed with a shear correction factor $\chi = 5/6$. Comparison with Table 4 shows that the use of reduced elastic coefficients provides improved

Table 5: First eight frequency parameters $\lambda = \omega R_o^2\sqrt{\rho h/D}$ of annular plates with $R_o = (10/3)R_i$, $h/R_o = 0.2$ and various boundary conditions. Results obtained by imposing $\sigma_{zz} = 0$ in HOT_1.

	Mode							
BC	1	2	3	4	5	6	7	8
FS	4.5328	11.205	12.711	15.875	20.740	27.931	30.530	31.301
FF	4.6160	7.8878	11.126	15.146	15.659	18.778	26.674	27.279
FC	10.365	15.895	25.384	35.763	36.860	39.424	40.534	43.901
CC	30.146	30.878	33.775	39.638	47.999	48.220	52.997	57.793

results. However, except for the torsional modes, frequencies are now underestimated, as previously pointed out by So and Leissa [15].

Another illustrative example is referred to a completely free annular plate with $R_o/R_i = 2$ and two different thickness-to-outer-radius ratios, $h/R_o = 0.4$ and $h/R_o = 1$. The first four non-dimensional frequencies $\lambda = \omega R_o\sqrt{\rho/G}$ corresponding to antisymmetric modes are shown in Table 6 for circumferential wavenumber n ranging from 0 to 3. Present solutions, computed with $M = 30$ and based on kinematic theories of order $N = 3$ and $N = 6$, are compared with the 3-D Ritz series solutions available in [15]. Similar conclusions to those outlined in the previous example can be drawn. In particular, it can be observed that a kinematic theory of moderate refinement ($N = 3$) is largely acceptable in providing accurate frequency solutions in the case of $h/R_o = 0.4$ over the whole frequency range considered in the comparison study. However, when relatively high-order modes of very thick plates are of interest, a 2-D kinematic theory of high refinement is required to achieve a high degree of accuracy. This is evident by examining the third and fourth modes corresponding to $n = 0$ when $h/R_o = 1$.

The last assessment involves an annular circular plate with an inner-to-outer-radius ratio $R_o/R_i = 5.0$ and a thickness-to-radius ratio $h/R_o = 0.5$. In this comparison study, the first 40 frequency parameters of antisymmetric and symmetric modes corresponding to circumferential wavenumbers $n = 0, 1, 2, 3$ are computed for two boundary conditions: a plate with free inner edge and clamped outer edge (FC), and a plate with both edges clamped (CC). Figures 2 and 3 show the percentage differences with respect to 3-D results given in [17] expressed by

$$\Delta\% = \frac{(\text{2-D frequency})_N - (\text{3-D frequency})}{(\text{3-D frequency})} \times 100 \tag{31}$$

where (2-D frequency)$_N$ refers to a frequency solution based on a refined 2-D theory of order N. In particular, comparison with 3-D analysis is given when $N = 3, 4, 5$ and 6 is adopted. Graphical results clearly show, in both cases, that HOT_3 gives reasonably accurate frequencies (differences within 2.5%) when the radial mode number s for each n is less than 10. Serious disagreement is observed for higher values of the wavenumber, unless the 2-D kinematic model is suitably enriched with additional

Table 6: Frequency parameters $\lambda = \omega R_o \sqrt{\rho/G}$ for the first four antisymmetric modes of completely free annular plates with $R_o = 2R_i$.

h/R_o	n	Method	Mode 1	2	3	4
0.4	0^a	Present ($N=3$)	1.388	8.344	9.167	14.498
		Present ($N=6$)	1.388	8.321	9.127	14.133
		3D-Ritz [15]	1.388	8.321	9.127	14.133
	1	Present ($N=3$)	1.944	8.049	8.554	8.974
		Present ($N=6$)	1.943	8.039	8.534	8.945
		3D-Ritz [15]	1.943	8.039	8.534	8.945
	2	Present ($N=3$)	0.691	3.127	8.422	8.814
		Present ($N=6$)	0.691	3.123	8.400	8.793
		3D-Ritz [15]	0.691	3.123	8.400	8.793
	3	Present ($N=3$)	1.681	4.459	8.834	9.007
		Present ($N=6$)	1.680	4.450	8.808	8.986
		3D-Ritz [15]	1.680	4.450	8.808	8.986
1	0^a	Present ($N=3$)	1.984	6.129	9.360	10.411
		Present ($N=6$)	1.984	5.775	8.329	9.355
		3D-Ritz [15]	1.984	5.772	8.258	9.084
	1	Present ($N=3$)	2.002	3.939	6.145	7.959
		Present ($N=6$)	1.999	3.930	5.842	7.719
		3D-Ritz [15]	1.999	3.930	5.839	7.706
	2	Present ($N=3$)	1.040	2.858	5.213	6.424
		Present ($N=6$)	1.039	2.846	5.173	6.160
		3D-Ritz [15]	1.039	2.846	5.172	6.157
	3	Present ($N=3$)	2.326	3.975	6.521	7.072
		Present ($N=6$)	2.320	3.947	6.393	6.808
		3D-Ritz [15]	2.320	3.946	6.392	6.805

higher-order terms. Except for some axisymmetric modes at very high frequency in the CC case, a substantial invariance of the degree of accuracy with respect to 3-D values is obtained when $N \geq 5$. Note also that, for each vibration category n, the discrepancy between 3-D results and 2-D solutions exhibits an overall increasing mean trend, but locally the percentage difference can be strongly dependent on the mode type. This is seen for example for modes $(n, s) = (3, 20)$ and $(3, 26)$ in Fig. 2 in the case $N = 3$. The present behaviour is more pronounced when theories of low order are used.

5 Conclusions

A novel variable-kinematic Ritz formulation capable of handling in an unified way an entire class of 2-D higher-order kinematic theories for accurate vibration analysis of circular and annular plates of any thickness has been derived. The method relies on suitable expansion of invariant kernels of the mass and stiffness matrix. The invariance is to be intended with respect to both the order of the theory and the type of Ritz trial functions. Considering the circumferential symmetry of the problem under study, the present method is computationally efficient even if kinematic models of high order are used.

Upper-bound frequency values have been presented using products of boundary-compliant functions and Chebyshev polynomials. It has been shown that the method exhibits good convergence properties and high numerical stability. As expected, increasing accuracy towards 3-D values in terms of frequency parameters has been found with theory refinement. Kinematic plate models of lower order are more sensitive to thickness-to-radius ratio, whereas accuracy is substantially independent from the plate thickness when a highly refined theory is adopted. This conclusion is also valid with reference to the frequency range of interest. Two examples have been provided to show the importance of refined models in the numerical evaluation of higher vibration modes.

References

[1] K.M. Liew, Y. Xiang, S. Kitipornchai, “Research on thick plate vibration: a literature survey”, Journal of Sound and Vibration, 180, 163-176, 1995.

[2] K.H. Lo, R.M. Christensen, E.M. Wu, “A high-order theory of plate deformation - part 1: homogeneous plates”, Journal of Applied Mechanics, 44, 663-668, 1977.

[3] M. Levinson, “An accurate, simple theory of the statics and dynamics of elastic plates”, Mechanics Research Communications, 7, 343-350, 1980.

[4] T. Kant, “Numerical analysis of thick plates”, Computer Methods in Applied Mechanics and Engineering, 31, 1-18, 1982.

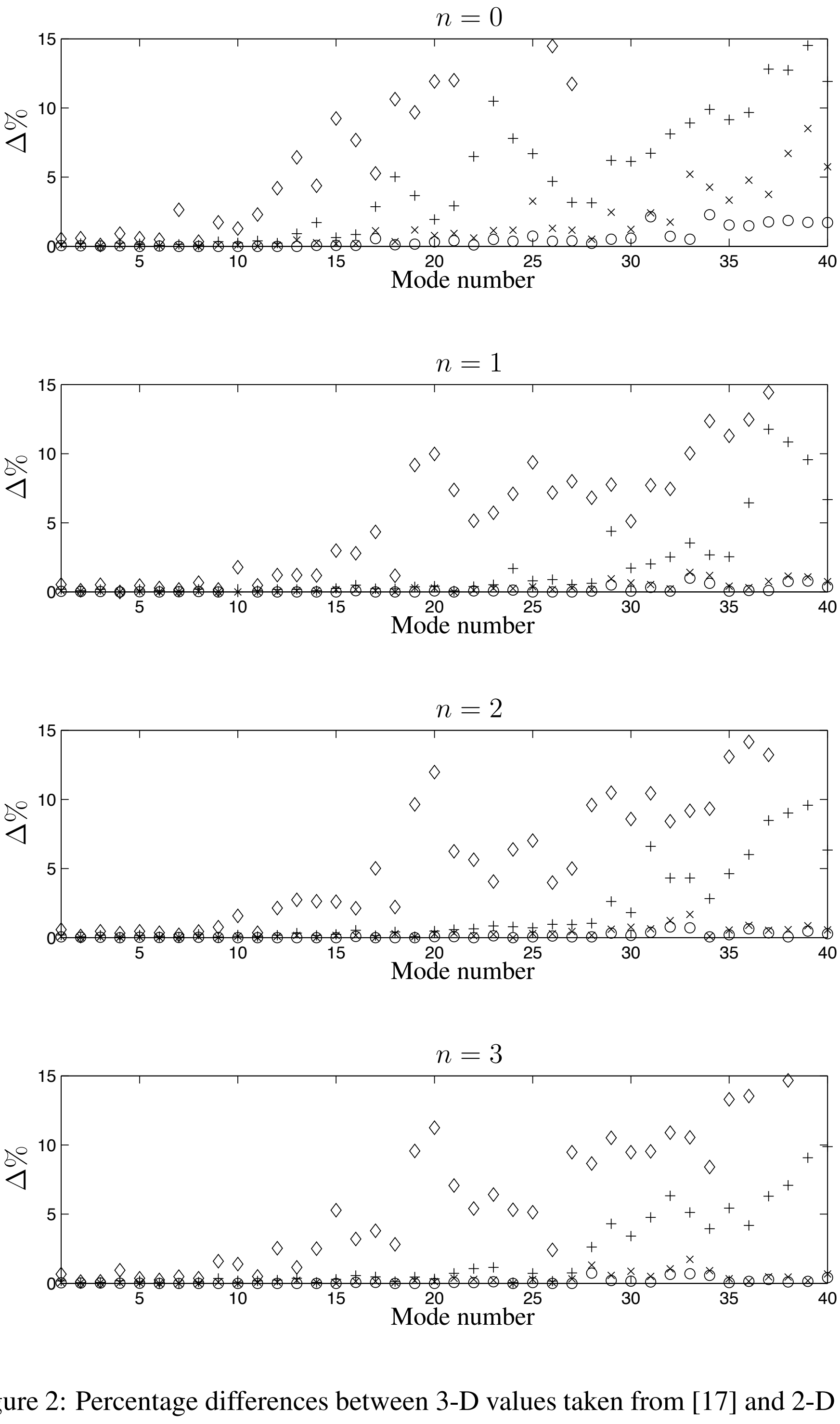

Figure 2: Percentage differences between 3-D values taken from [17] and 2-D present solutions based on refined theories of different orders for the first 40 modes with $n = 0, 1, 2, 3$ of an annular plate with free inner edge and clamped outer edge, $h/R_o = 0.5$ and $R_o = 5R_i$. Legend: $\diamond$, $N = 3$; $+$, $N = 4$; $\times$, $N = 5$; $\circ$, $N = 6$.

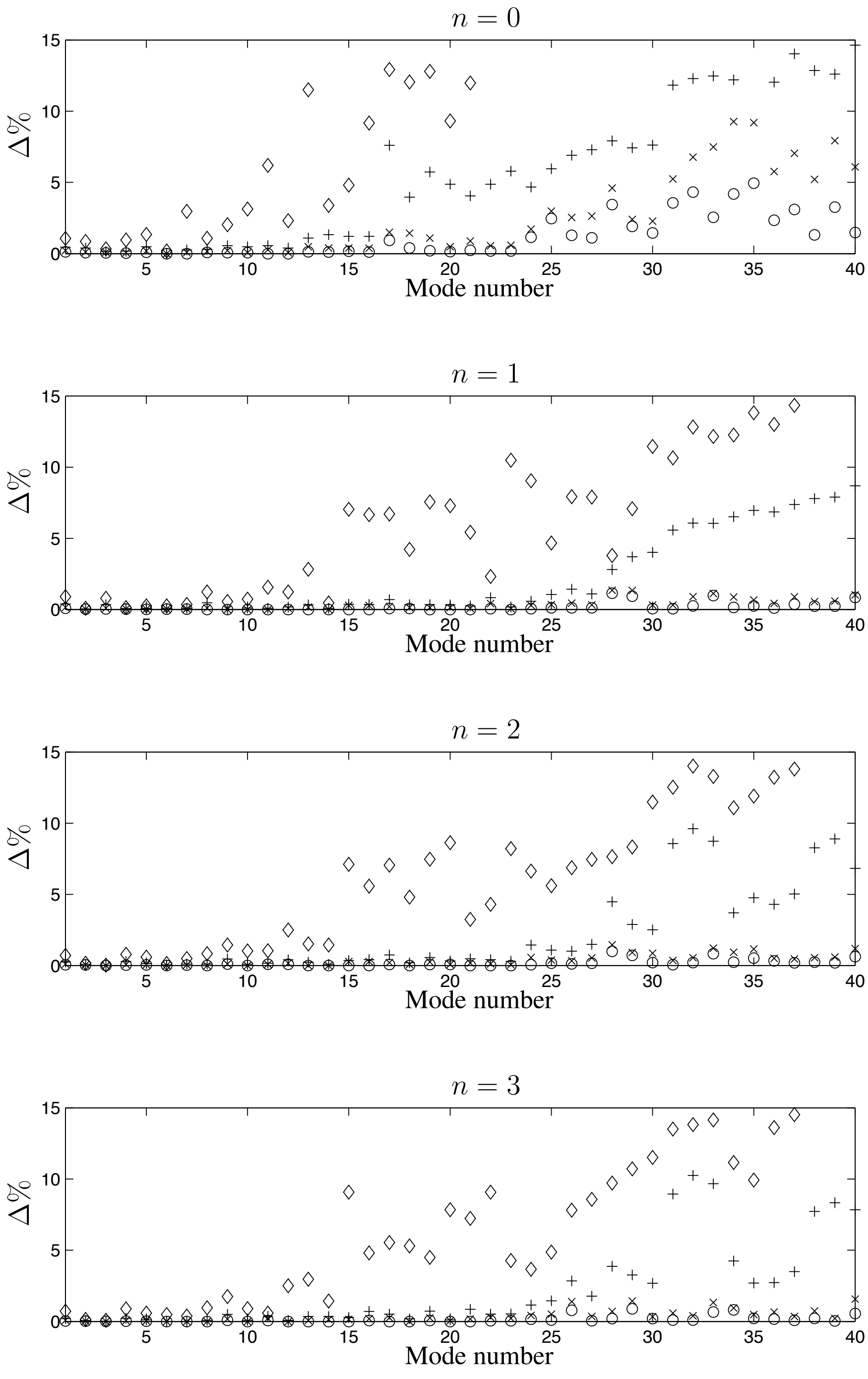

Figure 3: Percentage differences between 3-D values taken from [17] and 2-D present solutions based on refined theories of different orders for the first 40 modes with $n = 0, 1, 2, 3$ of an annular plate with both inner and outer edges clamped, $h/R_o = 0.5$ and $R_o = 5R_i$. Legend: $\diamond$, $N = 3$; $+$, $N = 4$; $\times$, $N = 5$; $\circ$, $N = 6$.

[5] J.N. Reddy, "A refined nonlinear theory of plates with transverse shear deformation", International Journal of Solids and Structures, 20, 881-896, 1984.
[6] N.F. Hanna, A.W. Leissa, "A higher order shear deformation theory for the vibration of thick plates", Journal of Sound and Vibration, 170, 545-555, 1994.
[7] H. Matsunaga, "Free vibration and stability of thick elastic plates subjected to in-plane forces", International Journal of Solids and Structures, 31, 3113-3124, 1994.
[8] R.C. Batra, S. Aimmanee, "Vibrations of thick isotropic plates with higher order shear and normal deformable plate theories", Computers and Structures, 83, 934-955, 2005.
[9] A.W. Leissa, "Vibration of plates", NASA SP-160, Office of Technology Utilization, Washington, 1969.
[10] Y. Narita, A.W. Leissa, "Flexural vibrations of free circular plates elastically constrained along parts of the edge", International Journal of Solids and Structures, 17, 83-92, 1981.
[11] M. Amabili, R. Pierandrei, G. Frosali, "Analysis of vibrating circular plates having non-uniform constraints using the modal properties of free-edge plates: application to bolted plates", Journal of Sound and Vibration, 206, 23-38, 1997.
[12] T. Irie, G. Yamada, K. Takagi, "Natural frequencies of circular plates", Journal of Applied Mechanics, 47, 652-655, 1980.
[13] K.M. Liew, J.B. Han, Z.M. Xiao, "Vibration analysis of circular Mindlin plates using the differential quadrature method", Journal of Sound and Vibration, 205, 617-630, 1997.
[14] J.R. Hutchinson, "Vibration of thick free circular plates, exact versus approximate solutions", Journal of Applied Mechanics, 51, 581-585, 1984.
[15] J. So, A.W. Leissa, "Three-dimensional vibrations of thick circular and annular plates", Journal of Sound and Vibration, 209, 15-41, 1998.
[16] K.M. Liew, B. Yang, "Elasticity solutions for free vibrations of annular plates from three-dimensional analysis", International Journal of Solids and Structures, 37, 7689-7702, 2000.
[17] D. Zhou, F.T.K. Au, Y.K. Cheung, S.H. Lo, "Three-dimensional vibration analysis of circular and annular plates via the Chebyshev-Ritz method", International Journal of Solids and Structures, 40, 3089-3105, 2003.
[18] Sh. Hosseini-Hashemi, H. Rokni Damavandi Taher, M. Omidi, "3-D free vibration analysis of annular plates on Pasternak elastic foundation via p-Ritz method", Journal of Sound and Vibration, 311, 1114-1140, 2008.
[19] L.W. Chen, J.R. Hwang, "Vibrations of initially stressed thick circular and annular plates based on a high-order plate theory", Journal of Sound and Vibration, 122, 79-95, 1988.
[20] Sh. Hosseini-Hashemi, M. Es'haghi, H. Rokni Damavandi Taher, M. Fadaie, "Exact closed-form frequency equations for thick circular plates using a third-order shear deformation theory", Journal of Sound and Vibration, 329, 3382-3396, 2010.
[21] H. Bisadi, M. Es'haghi, H. Rokni Damavandi Taher, M. Ilkhani, "Benchmark

solution for transverse vibration of annular Reddy plates", International Journal of Mechanical Sciences, 56, 35-49, 2012.

[22] L. Dozio, E. Carrera, "A variable kinematic Ritz formulation for vibration study of quadrilateral plates with arbitrary thickness", Journal of Sound and Vibration, 18-19, 4611-4632, 2011.

[23] L. Dozio, E. Carrera, "Ritz analysis of vibrating rectangular and skew multilayered plates based on advanced variable-kinematic models", Composite Structures, 94, 2118-2128, 2012.

[24] L. Dozio, "Natural frequencies of sandwich plates with FGM core via variable-kinematic 2-D Ritz models", Composite Structures, 96, 561-568, 2013.

[25] L. Dozio, "Computation of Eigenvalues for Thick and Thin Circular and Annular Plates Using a Unified Ritz-Based Formulation", *Proceedings of the Eleventh International Conference on Computational Structures Technology*, B.H.V. Topping, (Editor), Civil-Comp Press, Stirlingshire, United Kingdom, paper 96, 2012. doi:10.4203/ccp.99.96

[26] E. Carrera, "A class of two dimensional theories for multilayered plates analysis", Atti Accademia delle Scienze di Torino, Memorie Scienze Fisiche, 49-87, 1995.

Appendix A

By introducing the following thickness integrals

$$E_{\tau s} = \int_{-h/2}^{+h/2} F_\tau(z) F_s(z) \mathrm{d}z \qquad E_{\tau s_{,z}} = \int_{-h/2}^{+h/2} F_\tau(z) \frac{\mathrm{d}F_s(z)}{\mathrm{d}z} \mathrm{d}z$$

$$E_{\tau_{,z} s} = \int_{-h/2}^{+h/2} \frac{\mathrm{d}F_\tau(z)}{\mathrm{d}z} F_s(z) \mathrm{d}z \qquad E_{\tau_{,z} s_{,z}} = \int_{-h/2}^{+h/2} \frac{\mathrm{d}F_\tau(z)}{\mathrm{d}z} \frac{\mathrm{d}F_s(z)}{\mathrm{d}z} \mathrm{d}z$$

the matrices $\mathbf{Z}_{\tau s}^{\mathrm{pp}}, \ldots, \mathbf{Z}_{\tau s}^{\rho}$ in Eqs. (25) and (26) are defined as follows:

$$\begin{aligned}
\mathbf{Z}_{\tau s}^{\mathrm{pp}} &= E_{\tau s} \mathbf{C}_{\mathrm{pp}} & \mathbf{Z}_{\tau s}^{\mathrm{pn}} &= E_{\tau s} \mathbf{C}_{\mathrm{pn}} \\
\mathbf{Z}_{\tau s}^{\mathrm{np}} &= E_{\tau s} \mathbf{C}_{\mathrm{np}} & \mathbf{Z}_{\tau s}^{\mathrm{nn}} &= E_{\tau s} \mathbf{C}_{\mathrm{nn}} \\
\mathbf{Z}_{\tau s_{,z}}^{\mathrm{pn}} &= E_{\tau s_{,z}} \mathbf{C}_{\mathrm{pn}} & \mathbf{Z}_{\tau s_{,z}}^{\mathrm{nn}} &= E_{\tau s_{,z}} \mathbf{C}_{\mathrm{nn}} \\
\mathbf{Z}_{\tau_{,z} s}^{\mathrm{np}} &= E_{\tau_{,z} s} \mathbf{C}_{\mathrm{np}} & \mathbf{Z}_{\tau_{,z} s}^{\mathrm{nn}} &= E_{\tau_{,z} s} \mathbf{C}_{\mathrm{nn}} \\
\mathbf{Z}_{\tau_{,z} s_{,z}}^{\mathrm{nn}} &= E_{\tau_{,z} s_{,z}} \mathbf{C}_{\mathrm{nn}} & \mathbf{Z}_{\tau s}^{\rho} &= E_{\tau s} \rho
\end{aligned}$$

Appendix B

After introducing the quantities

$$\Gamma_c = \int_0^{2\pi} \cos^2(n\theta)\mathrm{d}\theta \qquad\qquad (n = 0, 1, 2, \dots)$$

$$\Gamma_s = \int_0^{2\pi} \sin^2(n\theta)\mathrm{d}\theta \qquad\qquad (n = 0, 1, 2, \dots)$$

and defining the following integrals

$$I_{\alpha\beta}^{abc} = \int_{-1}^{+1} \frac{\mathrm{d}^a\phi_{\alpha\tau i}}{\mathrm{d}\xi^a}\frac{\mathrm{d}^b\phi_{\beta sj}}{\mathrm{d}\xi^b}\,(\xi+\delta)^c\,\mathrm{d}\xi$$

the elements of the stiffness fundamental nucleus $\mathbf{K}_{\tau sij}$ can be explicitly written as follows:

$$\begin{aligned}
K_{\tau sij}(1,1) &= E_{\tau s}C_{11}\,\Gamma_c I_{\xi\xi}^{111} + E_{\tau s}C_{22}\,\Gamma_c I_{\xi\xi}^{00-1} + E_{\tau s}C_{12}\,\Gamma_c\left(I_{\xi\xi}^{100} + I_{\xi\xi}^{010}\right)\\
&\quad + E_{\tau s}C_{66}\,n^2\,\Gamma_s I_{\xi\xi}^{00-1} + E_{\tau_{,z}s_{,z}}C_{55}\,\gamma^2\,\Gamma_c I_{\xi\xi}^{001}\\
K_{\tau sij}(1,2) &= E_{\tau s}C_{12}\,n\,\Gamma_c I_{\xi\theta}^{100} + E_{\tau s}C_{22}\,n\,\Gamma_c I_{\xi\theta}^{00-1} + E_{\tau s}C_{66}\,n\,\Gamma_s\left(I_{\xi\theta}^{00-1} - I_{\xi\theta}^{010}\right)\\
K_{\tau sij}(1,3) &= E_{\tau s_{,z}}C_{13}\,\gamma\,\Gamma_c I_{\xi z}^{101} + E_{\tau s_{,z}}C_{23}\,\gamma\,\Gamma_c I_{\xi z}^{000} + E_{\tau_{,z}s}C_{55}\,\gamma\,\Gamma_c I_{\xi z}^{011}\\
K_{\tau sij}(2,1) &= E_{\tau s}C_{12}\,n\,\Gamma_c I_{\theta\xi}^{010} + E_{\tau s}C_{22}\,n\,\Gamma_c I_{\theta\xi}^{00-1} + E_{\tau s}C_{66}\,n\,\Gamma_s\left(I_{\theta\xi}^{00-1} - I_{\theta\xi}^{100}\right)\\
K_{\tau sij}(2,2) &= E_{\tau s}C_{22}\,n^2\,\Gamma_c I_{\theta\theta}^{00-1} + E_{\tau s}C_{66}\,\Gamma_s\left(I_{\theta\theta}^{111} - I_{\theta\theta}^{100} - I_{\theta\theta}^{010} + I_{\theta\theta}^{00-1}\right)\\
&\quad + E_{\tau_{,z}s_{,z}}C_{44}\,\gamma^2\,\Gamma_s I_{\theta\theta}^{001}\\
K_{\tau sij}(2,3) &= E_{\tau s_{,z}}C_{23}\,n\gamma\,\Gamma_c I_{\theta z}^{000} - E_{\tau_{,z}s}C_{44}\,n\gamma\,\Gamma_s I_{\theta z}^{000}\\
K_{\tau sij}(3,1) &= E_{\tau_{,z}s}C_{13}\,\gamma\,\Gamma_c I_{z\xi}^{011} + E_{\tau_{,z}s}C_{23}\,\gamma\,\Gamma_c I_{z\xi}^{000} + E_{\tau s_{,z}}C_{55}\,\gamma\,\Gamma_c I_{z\xi}^{101}\\
K_{\tau sij}(3,2) &= E_{\tau_{,z}s}C_{23}\,n\gamma\,\Gamma_c I_{z\theta}^{000} - E_{\tau s_{,z}}C_{44}\,n\gamma\,\Gamma_s I_{z\theta}^{000}\\
K_{\tau sij}(3,3) &= E_{\tau s}C_{55}\,\Gamma_c I_{zz}^{111} + E_{\tau s}C_{44}\,n^2\,\Gamma_s I_{zz}^{00-1} + E_{\tau_{,z}s_{,z}}C_{33}\,\gamma^2\,\Gamma_c I_{zz}^{001}
\end{aligned}$$

The non-null elements of the mass fundamental nucleus $\mathbf{M}_{\tau sij}$ are given by

$$\begin{aligned}
M_{\tau sij}(1,1) &= E_{\tau s}\rho\,\gamma^2\,\Gamma_c I_{\xi\xi}^{001}\\
M_{\tau sij}(2,2) &= E_{\tau s}\rho\,\gamma^2\,\Gamma_s I_{\theta\theta}^{001}\\
M_{\tau sij}(3,3) &= E_{\tau s}\rho\,\gamma^2\,\Gamma_c I_{zz}^{001}
\end{aligned}$$

By setting $n = 0$ in the above equations, axisymmetric modes are obtained. Note that, in this case, $K_{\tau sij}(1,2) = K_{\tau sij}(2,1) = K_{\tau sij}(2,2) = K_{\tau sij}(2,3) = K_{\tau sij}(3,2) = 0$ and $M_{\tau sij}(2,2) = 0$.

In the case of torsional modes, the circumferential is once again null, but now Γ_c is replaced by Γ_s and conversely. Therefore, the only non-zero terms are the following:

$$K_{\tau sij} = E_{\tau s} C_{66}\, \Gamma_c \left(I_{\theta\theta}^{111} - I_{\theta\theta}^{100} - I_{\theta\theta}^{010} + I_{\theta\theta}^{00-1} \right) + E_{\tau,_z s,_z} C_{44}\, \gamma^2\, \Gamma_c I_{\theta\theta}^{001}$$

$$M_{\tau sij} = E_{\tau s} \rho\, \gamma^2\, \Gamma_c I_{\theta\theta}^{001}$$